Characterization of two-photon-polymerization lithography structures via Raman spectroscopy and nanoindentation

Severin Schweiger[a,b,*] **Tim Schulze**[a,b] **Simon Schlipf**[c] **Peter Reinig**[a] **and Harald Schenk**[a,b]

[a]Fraunhofer Institute for Photonic Microsystems, Dresden, Germany
[b]Brandenburg University of Technology, Cottbus, Germany
[c]Fraunhofer Institute for Ceramic Technologies and Systems, Dresden, Germany

Abstract. Additive manufacturing using two-photon polymerization (TPP) lithography is increasingly used in industry and research. Parameter sweeps of cuboid structures fabricated using TPP lithography were investigated across the parameters of the laser power and scan speed to find dependent mechanical material properties. The employed photoresists were examined using Raman spectroscopy to find the degree of conversion (DC) of monomer to polymer, and subsequently, micro- or nanoindentation was used to find Young's modulus (E). For the photoresist IP-Dip, the attained DC and E ranged from 20% to 45% and 1 to 2.1 GPa, respectively. The results were compared with reports found in the literature. For IP-Q, the attained DC and E ranged from 53% to 80% and 0.5 to 1.3 GPa, respectively. The characterized properties of IP-Q manifest as the current state of knowledge of the material. [DOI: 10.1117/1.JOM.2.3.033501]

Keywords: two-photon polymerization; Raman spectroscopy; nanoindentation.

Paper 22012G received May 25, 2022; accepted for publication Jul. 11, 2022; published online Aug. 10, 2022.

1 Introduction

Two-photon polymerization lithography (TPP)[1] is an additive manufacturing process growing in recognition and usage for applications in various fields. TPP is based on selective curing of a liquid precursor to create solid structures. Its large scale of addressable dimensions from micro to macroyields the mentioned applicability, especially because new materials are available.

Well-known TPP applications are optical submicron structures[2] in which the photoresists IP-Dip and IP-L (Nanoscribe GmbH, Germany) are commonly utilized. The more recently developed photoresist IP-Q was designed by the same manufacturer for larger size applications, e.g., mounts,[3] molds,[4] and structural metamaterials.[5]

Currently, a major constraint of TPP in general and specifically IP-Q is that users have limited access to knowledge about material properties. For example, before this work, no degree of conversion (DC) and Young's modulus values for IP-Q have been reported. Due to the nature of the process, the elastic properties, especially, depend not only on the utilized material but on structure size, process parameters, and hatch strategy.[6] The latter represents the arrangement and order of points to which the fabrication laser moves in succession.

Standardized strain rate-dependent testing methods for elastic properties are usually difficult to apply to the size of structures that can be fabricated via TPP within a reasonable timeframe. For this work, the micro- and nanoindentation method was chosen because it is a more straightforward method for small structures when compared with microtensile experiments.[7–10] One reason for this is the less intensive sample preparation, whereas the design and fabrication of microtensile experiments can become complicated and time-consuming. Furthermore, the

*Address all correspondence to Severin Schweiger, severin.schweiger@ipms.fraunhofer.de

indentation method can be easily automated, allowing for a more reasonable timeframe for characterization.

The approach applied in Refs. 6 and 11 uses a combination of Raman spectroscopy and nanoindentation to characterize photoresists IP-Dip and IP-L. In these references, the DC of monomer to polymer measurable via Raman spectroscopy was then related to the mechanical behavior of the material, measurable via nanoindentation.[12]

Knowledge of the mechanical properties deduced from Raman spectroscopy allows for the non-destructive characterization of structures that would otherwise be too small or of structure parts with dimensions and shapes that do not allow for standard hatch strategies. Furthermore, the method can help recognize suitable parameter spaces for the fabrication of the intended mechanical behavior. Previously, efforts were undertaken to realize in-situ monitoring of the TPP process with Raman spectroscopy.[13]

Current research on acoustic metagratings[14] and metamaterials fabricated on MEMS[15] would benefit from optimized elastic parameters to provide adjustability of the acoustic behavior as they affect the characteristic acoustic impedance directly. In this work, we employ the method described in Ref. 6 to characterize samples fabricated from IP-Q and IP-Dip using TPP via Raman spectroscopy and micro- and nanoindentation.

2 Materials and Methods

The liquid negative tone photoresists IP-Dip and IP-Q investigated in this work consist of organic monomers, solvents, and radical photoinitiators. The latter can create radical species upon exposure to UV radiation. The former react in contact with these free radicals, initiating the polymerization. Short monomers link to form chains, which cross-link to form networks. As the lengths of the chains and the entanglement of the networks increase with the number of such reactions, the former liquid becomes gel-like and subsequently solid.

The concentration of radicals is dependent on the exposure dose of UV radiation, as is the DC. It denotes the ratio of monomer left in a volume to the amount of polymer. The larger the exposure dose is, the higher the DC is, and the stronger the entanglement and cross-linking are, which consequently forecast the mechanical properties of the polymerized photoresist.

The reactive monomer of IP-Dip is acrylic based, whereas withIP-Q, methacrylates are used.[16] They can respond to the mentioned radical polymerization and were specialized for exposure using TPP. IP-Dip was intended for microfabrication with a priority on high resolution, and IP-Q was intended for meso to macrofabrication with a priority on fabrication speed.[17]

2.1 *Two-Photon Polymerization Lithography*

Cuboid parameter sweep samples were fabricated using additive manufacturing based on TPP, which takes advantage of two-photon absorption.[18] This process was carried out using the Photonic Professional GT2 system (Nanoscribe GmbH, Germany). Within it, a focused and pulsed laser beam invokes a multiple photon absorption process inside a volume of a photoresist containing appropriate photoinitiators. The absorption of a first photon creates a virtual state, from which the following photon initiates the excited state necessary to induce the curing reaction within the focal volume (voxel, three-dimensional pixel). The voxel shape and its size depend on the exposure dose and the employed objective. A radial and vertical size of ~0.1 to 5 and 0.3 to 15 μm can be addressed this way, respectively.

The sample structures were created by scanning the voxel through the photoresist following positional data from programmed machine code including a hatch strategy. Common strategies lead to a concentrated intensity distribution at the start and end points of the hatch lines, where the galvanometer mirrors directing the laser beam have to accelerate and decelerate, leading to dose variations. Here, each layer of a cuboid is identical, and each hatch line starts on one edge and ends at the opposing edge. In this way, the inconsistencies occur outside the area designated for characterization.

The exposure dose depends on the swept parameters, as well as on the material properties of the resist and substrate[19] and the TPP setup. Structures become corrupted when the dose exceeds

the overexposure threshold or falls below the underexposure threshold. The latter describes the minimum dose to polymerize structures that withstand the processing until characterization. The former is due to ionization and/or the excess heat of the photothermal process, which can vaporize the solvents present in the resist.[19–22] Both thresholds also appear as boundaries for the measurable DC.

Each cuboid of the parameter sweeps represents a different combination of the laser power (rows, x-direction) and scan speed (columns, y-direction). A preceding sweep was carried out, including the minimum and maximum laser power of 0 to 50 mW at the objective lens, to find viable settings per respective scan speed, whereas the latter was stepped through the processable range. Under- and overexposed samples were left out in the subsequent sweep designated for characterization, leading to a different step size and start value for each row.

Focusing was conducted by means of immersion objectives 10× numerical aperture (NA 0.3) and 63× (NA 1.4) for resists IP-Q and IP-Dip, respectively. The substrates used in this work were silicon wafer dies of 725-μm thickness. Excess photoresist was removed in a development step after the parameter sweep fabrication had been completed, leaving the cured structures. The development agents 1-Methoxy-2-propyl acetate (20 min, 60 mL) and 2-propanol (5 min, 60 ml) were used. The samples were dried in air at (21.7 ± 0.44)°C and (32.1 ± 8.2)% relative humidity under a glass hood.

2.2 *Raman Spectroscopy*

Raman spectroscopy was performed at room temperature using the confocal Raman microscope inVia Qontor (Renishaw plc) with a laser operating at a 785-nm wavelength and employing a DM2700 microscope (Leica Camera AG) with a 100× NPLAN-objective lens. Measurements were conducted in the Stokes-regime using a Rayleigh filter with 100 cm^{-1} cut-off wavenumber. The spectral resolution of the system is <1.0 cm^{-1} for the full width at half maximum, with a long-term spectral stability of $< \pm 0.05$ cm^{-1}. This is highly accurate considering the samples under investigation. Raman spectra acquisition was conducted at an exposure time of 10 s per individual spectrum and an integration of six subsequent individual measurements. After the acquisition of the raw spectra, a baseline correction was performed.

The polymerization of monomers entails the conversion of carbon double bonds (C=C) to carbon single bonds (C—C).

Raman spectroscopy of IP-Q shows prominent peaks at 1637 and 1737 cm^{-1} attributed to the vibrational modes of the C=C and carbonyl (C=O) groups;[23] see Fig. 1(b). The ratio of the integrated peak intensity of C=C changes with the DC. The corresponding ratio of C=O does not and, thus, can be employed as a reference for the calculation of the DC. The DC of each cuboid was evaluated from the measured Raman spectra using the equation described in Ref. 11:

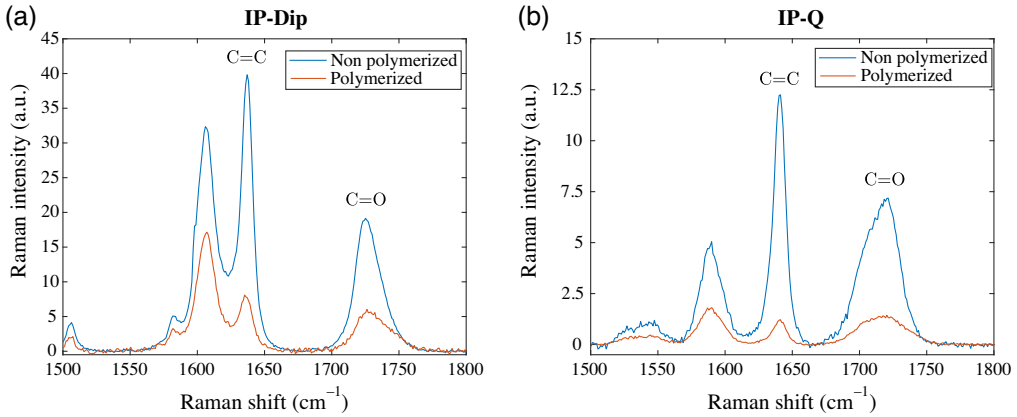

Fig. 1 Raman spectra of non-polymerized and polymerized photoresist IP-Dip (a) and the same for photoresist IP-Q (b) with C=C and C=O labels indicating the respective vibrational modes.

$$\mathrm{DC}[\%] = 100 \cdot \left[1 - \left(\frac{A_{C=C}/A_{C=O}}{A'_{C=C}/A'_{C=O}}\right)\right] \tag{1}$$

where $A'_{C=C}$ and $A'_{C=O}$ are the integrated intensities of the corresponding C=C and C=O peaks of unpolymerized photoresist, respectively (see Fig. 1). $A_{C=C}$ and $A_{C=O}$ are analogously referring to the polymerized photoresist, respectively. The prominent peak IP-Dip at 1610 cm^{-1} [see Fig. 1(a)] is likely related to 9,9-bis(4-(2-acryloyloxyethyloxy)phenyl)fluorene as identified in Ref. 24. An automated peak fitting routine using a Gaussian function for the C=O peak and a Lorentzian function for the C=C peak was applied to find the individual peak positions. The integral calculation was achieved using the corresponding fit parameters to analytically calculate the area under each peak.

2.3 *Indentation*

Indentation measurements were conducted to locally determine the material properties, e.g., reduced Young's modulus E_r and hardness, of TTP structures. The relation of E_r to Young's modulus E and Poisson's ratio ν of the indenter tip material (subscript i) and the sample material (no subscript) was described in Refs. 25 and 26 as

$$E = (1-\nu^2)\left[\frac{1}{E_r} - \frac{(1-\nu_i^2)}{E_i}\right]^{-1}, \tag{2}$$

where E_i and ν_i of the indenter tip were set to 1.14 Tpa and 0.07, respectively. Indentation methods are commonly utilized to measure mechanical properties of thin films with thicknesses of some few hundred nanometers.[12] Here, indentation was used to test each TTP structure to spatially map the mechanical properties over the grid of a sweep. The measured load-displacement data of each indent and the previously calibrated contact area of a pyramidal shaped tip geometry were used to compute E_r and calculate E, via Eq. (2).[12,25,26] A Hysitron TI950 triboindenter (Bruker Corporation) equipped with a Berkovich tip was employed to locally load the sample specimen.

A rotational stage was utilized to align the parameter sweep with the orientation of the linear stages of the indenter, to realize similar test conditions for each cuboid with indent locations in the center of the structure. The spatial resolution of the linear stage of up to 500 nm was then used to step through each specimen. To measure over a representative sample volume, nano- and microindentation measurements were carried out using two different transducers. The two indentation testing routines for the smaller IP-Dip and larger IP-Q structures were established in an experimental study, see Fig. 2.

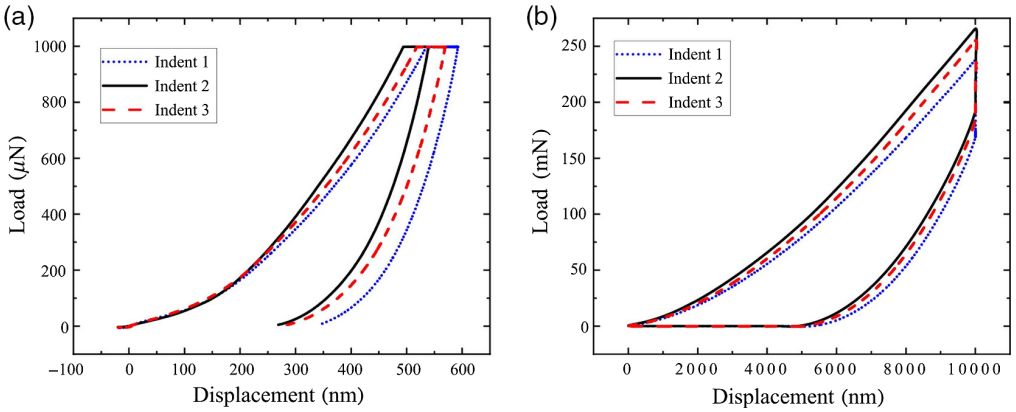

Fig. 2 Force limited nanoindentation measurement of a cuboid structure fabricated from IP-Dip (a) and an indentation depth limited microindentation measurement of a cuboid structure fabricated from IP-Q (b), respectively.

For the IP-Dip samples, the nanoindentation method was selected and the load-displacement data were evaluated at three different locations in the center of the structure, followed by averaging. The maximum viable force of the high precision transducer was the limit, as visualized in Fig. 2(a). The loading rate was 66.67 μN/s, and the force was applied from 250 to 1000 in steps of 250 μN.

For the IP-Q samples, the high-load microindentation transducer with a maximum contact load of up to 1.4 N was selected, and indentations were performed at four locations in the center of the structures, before averaging. The measurement was limited to a depth of 10 μm; see Fig. 2(b). The loading rate was 15.63 mN/s, and the force was applied from 5 to 250 in steps of 5 mN.

Previously conducted nanoindentation measurements on IP-Q samples with indentation depths of some few hundred nanometers resulted in strongly diverging material properties compared with the measurements with micrometer indentation depths. A parametric load variation study was conducted on two representative IP-Q samples to identify suitable contact loads and displacements for the experimental study. The evaluation of E as a function of indentation depth indicated preferable conditions with stable mechanical properties for depths in the range of 10% of the total structure height, which is commonly recommended for indentation testing on thin films to avoid the influence of the significantly stiffer substrate.[12] The identified indentation parameters were subsequently applied to test each individual cuboid of the parameter sweep using a displacement-controlled loading function at a depth of 10 μm. An automated method based on the pitch and sample size of the sweep field was implemented.

3 Results

Cuboid parameter sweeps with 10×10 elements were fabricated from IP-Dip and IP-Q. The cuboid dimensions were $(20 \times 20 \times 20)$ μm^3 and $(500 \times 500 \times 100)$ μm^3, respectively.

The samples were imaged using a FlexSEM 1000 II (Hitachi, Ltd.) scanning electron microscope. Figure 3(a) shows the sweep of IP-Q, and it can be seen that some of the cuboids of the bottom right quadrant are larger in height than the others and are deformed at the top, where the cuboid morphs into a pillow shape.

Each specimen was fabricated with a text element fabricated next to it that contained information about the laser power and scan speed; see Fig. 3(b). The same micrograph shows an example cuboid fabricated from IP-Dip at parameters that lead to overexposure. This is evident from the crater on the top surface of the cuboid, which stems from a bubble of vaporized photoresist that prevented the curing of monomer in its place. The micrograph also reveals the voxel shape and hatch line configuration, upon closer examination.

From the fabricated 10×10 sets of IP-Dip and IP-Q cuboids, an example subset of selected scan speed settings is shown in Fig. 4, where the measured DC and E values were plotted over the laser power. The cuboids with the respective scan speed settings of 100, 70, 10, and 1 mm/s were fabricated with laser power settings of the first cuboid and the laser power step

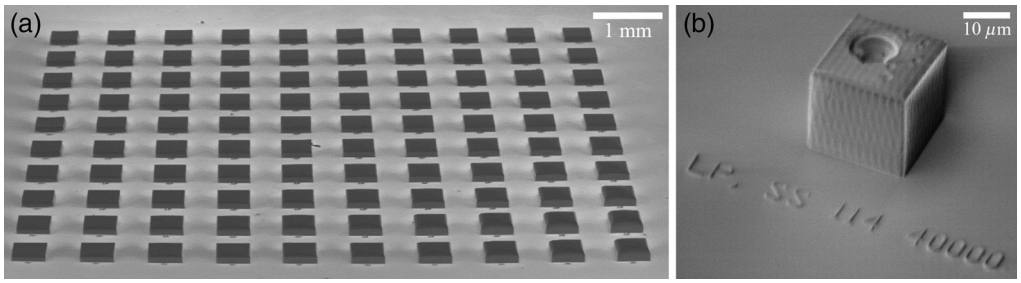

Fig. 3 (a) A 60-deg tilted view SEM micrograph of a cuboid parameter sweep comprising 10×10 elements fabricated via TPP from the photoresist IP-Q and (b) 60-deg tilted and 30-deg rotated view SEM micrograph of a single cuboid fabricated via TPP from the photoresist IP-Dip showing evidence of overexposure.

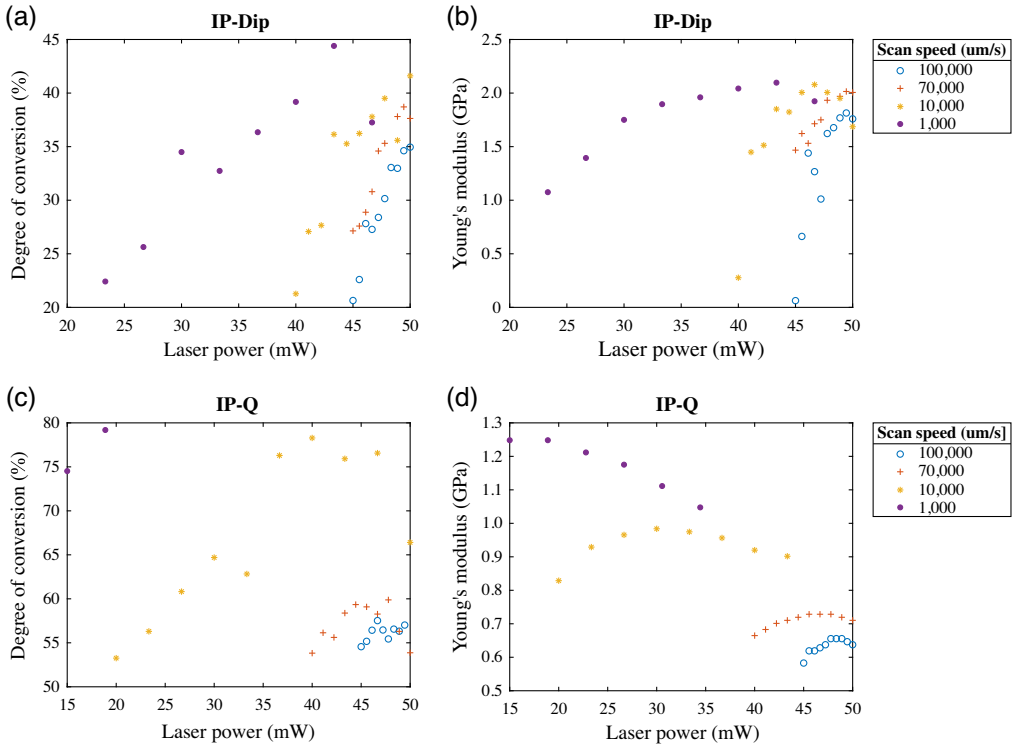

Fig. 4 (a) Scatter plot of the DC and (b) E dependence of IP-Dip cuboids on the laser power for selected scan speeds and (c) the same for the DC and (d) E dependence of IP-Q cuboids, for which the indentation measurements of the chosen IP-Q and IP-Dip samples have a relative standard deviation averaged to 2.5% and 3.7%, respectively.

size of 33, 33, 14, 7 mW and 3, 3, 3, 2 mW per step for IP-Dip. For IP-Q, they were fabricated using 45, 40, 20, 15 mW and 0.6, 1.1, 3.3, 3.9 mW per step.

Further selection was imposed by the requirement of a maximum of 5% relative standard deviation of the micro- or nanoindentation measurement and a minimum signal-to-noise ratio of the Raman spectroscopy measurements of >10.

Figure 4(a) shows the DC of cuboids fabricated from IP-Dip for various settings, and when compared with Fig. 4(b) showing Young's modulus, one can recognize the difference in deviation being larger for the DC. The expected correlation of DC and E with laser power is nonetheless viable; each rises with increasing laser power. The various scan speed settings shift the resulting properties as expected; a lower scan speed leads to an increased DC, as well as E.

The same cannot entirely be said for IP-Q. Figures 4(c) and 4(d) show the DC and E values rising with the laser power, respectively. But the relation reverses; the DC and E values drop even while the laser power increases. This behavior is more drastic with lower scan speeds, e.g., 1000 μm/s, in which the highest laser power setting results in the lowest E value. The lower scan speeds generally had the strongest distortions of shape; see Fig. 3(a). Most of the pillow-shaped cuboids were deselected due to large deviations or low signal-to-noise ratio, which leaves Fig. 4(c) with very few data points for a low scan speed specimen.

Previous studies of the elastic behavior of IP-Dip show varying settings and setups, but allow for comparison of the E values found so far; see Table 1. Further processing of structures fabricated via TPP can also have an effect on the resulting E values, e.g., UV flood curing[24] or thermal treatments.[29,30]

As shown in Fig. 5(a), starting with the smallest DC values of ~20%, the E value of the IP-Dip-based cuboids shows a strong spread around 1 GPa. The expected increasing trend continues to a maximum DC value of roughly 45%. As DC values increase, E values show an ever-decreasing spread and ultimately converge at ~2.1 GPa.

Table 1 Results of Young's modulus measurements of IP-Dip and respective settings found in the literature.

References	Young's modulus (GPa)	Laser power (mW)	Scan speed (μm/s)	Hatch/slice distance (μm)	Objective
Bauer et al.[6]	0.6...3.6	9...17	1000	0.1/0.05	63× (NA 1.4)
Lemma et al.[7]	~0.75...3.6	5...13	100	Unknown	100× (NA 1.4)
Meza et al.[27]	2.1 ± 0.3	9	50	Unknown	Unknown
Bauhofer et al.[28]	2.45 ± 0.2	16	55,000	0.3/0.5	25× (NA 0.8)
Rohbeck et al.[8]	2.58 ± 0.12	22	8000	0.2/0.2	63× (NA 1.4)

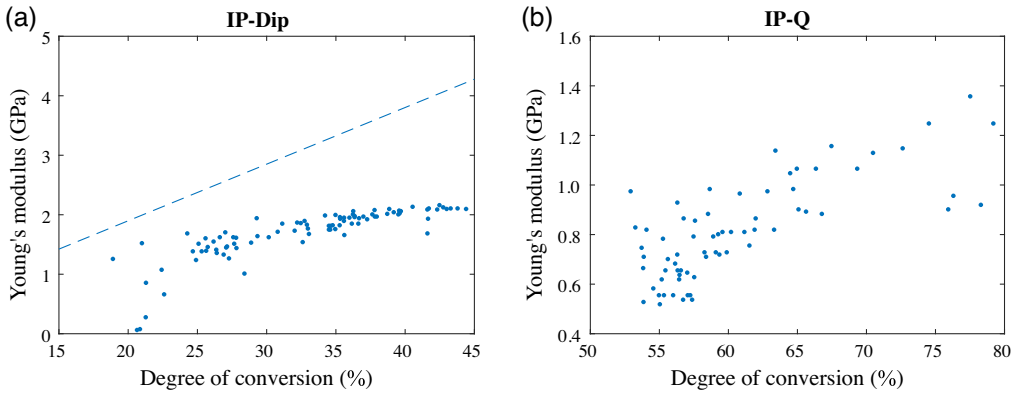

Fig. 5 Scatter plot of Young's modulus E of 92 viable IP-Dip-based cuboids in comparison with their corresponding DC value including (a) a dashed line with E = (9.52 DC − 0.56) GPa representing fitted data points from Ref. 6 and (b) a scatter plot of the E value of 68 viable IP-Q-based cuboids in comparison with their corresponding DC value. The indentation measurements of the IP-Q and IP-Dip samples have a relative standard deviation averaged to 2.5% and 3.7%, respectively.

Thus, exploiting the range of exposure doses achieved in this work, it is evident that only DC values between 20% and 45% were obtainable, which corresponds to the results for IP-Dip in Ref. 6. However, unlike prior work,[6] the E values obtained from this setup are significantly smaller and do not depict a linear increase. Furthermore, very low E values were measured at very low DC values.

A comparison of the E values of IP-Q-based cuboids with their corresponding DC values in Fig. 5(b) shows a similar relation for the case of IP-Dip-based cuboids [Fig. 5(a)]. However, over the DC value range of ~53% to 80%, E values increase monotonously with a range from roughly 0.5 to 1.3 GPa. Although the IP-Q-based cuboids obtain higher DC values, their E values are smaller compared with IP-Dip-based cuboids. Furthermore, the data points show a significant spread along all measured DC values, which prevents a trustworthy fit.

4 Discussion

The goal of this work was to provide insight to the transferability of the TPP-Raman-indentation method to a new material and to supply potentially useful material characteristics.

4.1 *IP-Dip*

For IP-Dip, a comparison of E values with the literature is viable as there are some previously report values [see Table 1 and Fig. 5(a)]. The linear correlation of the laser power to Young's

modulus reported in Ref. 7 might be due to the low maximum laser power setting, the differences in the measurement setup, and the differences in the fabrication setup.

The results found in Ref. 6 more closely resemble what was found in this work: E increases with laser power up to a point at which it asymptotically levels out. A lower hatch distance and slice height result in higher overall E values, however.

The 2.1 GPa reported for IP-Dip in Ref. 27 are comparable to the asymptotical convergence to 2.1 GPa found in this work, although the scan speed was lower than what was tested here and the other settings are unknown.

The exposure settings found in Refs. 8 and 28 are very different from what was realized here, probably due to the drastically smaller structure volume and different test environments and setups.

The difference between the DC versus E plot of IP-Dip [see Fig. 5(a)], when compared with the fit found in Ref. 6, are the generally lower values for E and the asymptotic approach to a maximum of approximately 2.1 GPa. Reasonable explanations are differences in the utilized material, i.e., batch variations, or the storage conditions. The materials employed in this work were used within their minimum storage life at ∼2 months after opening of the 3-g containers, which were stored at (8.0 ± 0.3)°C. None of these details were available in Ref. 6.

As mentioned in Sec. 2.1, the parameter sweeps were fabricated twice. The first set had laser power settings that sampled the whole available range. This resulted in some viable samples sandwiched between over- and underexposed samples, which were neglected for the subsequent sweep. Setting a maximum and minimum leads to bottom and top thresholds for the dose, the DC, and Young's modulus and can also explain the offset from measurements made in Ref. 6. Each minimum and maximum laser power setting was selected from the first sweep with a range of 5% and 10% steps for under- and overexposure, respectively. If the true threshold falls closer to the neglected laser power rather than the selected one, the deviation from the selected power would be at a maximum of 0.25 and 0.15 mW for under- and overexposure, respectively. Thus, the range of dose, DC, and Young's modulus could be increased by decreasing the step size between the elements of the initial sweep at the cost of increased fabrication time.

The error of the Raman DC measurement has systematic and random contributions. Both spectral resolution and spectral stability of the system are highly accurate considering the samples under investigation and can be neglected in this case. However, the estimated approximate error for the DC values is dominated by the specific peak fitting routine and was evaluated to an absolute value of 12%. This depended on the peak fitting procedure, with manual peak fitting resulting in increased DC values at the cost of increased characterization time.

Another reason for the mismatch could be differences in the fabrication of the samples. The hatch distance (the distance between laser lines) and slice height (the distance between layers) were not modulated in this work; they were set to 0.2 and 0.3 μm for IP-Dip and 1 and 5 μm for IP-Q, which is the standard recipe recommended by the manufacturer. A comparison of the asymptotic slope of Fig. 5(a) with the very similar behavior of the E versus laser power graphs in Fig. 4(b) and similar figures in Ref. 6 reinforces the assumption that the missing adjustable distances make the difference. Even higher E values could be viable when these parameters are adjusted and interact with fitting settings for scan speed and laser power. Furthermore, the hatch direction could be rotated per layer, which might be another reason for the differences in the literature.

The strong spread of the E values of the IP-Dip samples in the DC range of 20% to 25% could be explained by the generally low DC, which can lead to inconsistencies in polymerization across the volume. Partly connected hatch lines could lead to very low measured E values.[6] An indentation measurement between two hatch lines could show different results than when the voxel line is hit directly. The cuboids with the lowest E values were generally fabricated using the lowest laser power settings available, making them more inclined to fall into the underexposure regime.

The incident dose affects the size and shape of the voxel, and the same applies to the cuboid. Low dose examples shrink from their set height and reduce in footprint (visible in Fig. 3), except at the bottom, where they adhere to the substrate. The adhesion can lead to tension and subsequent detachment from the substrate.

High-dose examples that surpass their target height can also form cushion-shaped tops. This can lead to less stable indentation measurement conditions due to the inhomogeneous sample surface and, subsequently, increase deviation.

4.2 *IP-Q*

Many of the assertions made for IP-Dip most likely are valid for IP-Q as well, e.g., shrinkage, deformation, (partial) detachment, threshold selection, and dose correlation with hatch and slice distances. In the case of IP-Dip, the voxel size was small in comparison with the indentation depth. The opposite was true for the IP-Q samples, in which the larger voxel of the 10× objective seems to lead to a strong interference with the measurement. A deeper penetration depth had to be realized for the measurements to result in viable outputs that average the material characteristics.

With respect to the Raman evaluation of the IP-Q structures it has to be noted that the resulting Raman spectra were sensitive concerning the focal depth of the laser beam. To deduce the previously shown DC values, the Raman microscope was focused in the areal center and ideally about 30 μm below the top surface of each cuboid. However, deviations from the ideal cuboid structure or lateral variations of the surface height lead to focal point variations of the laser beam, which could only be partially accounted for in the semi-automated measurement procedure.

As a result, a part of the acquired Raman spectra showed reduced signal-to-noise ratio and thus had to be neglected for further evaluation. The affected set generally belonged to the high dose samples, which would entail that the evaluated maxima of the DC and E values of the set considered for the end result are reduced from the actual values of the total set.

This finding was also confirmed via additional depth scans in 10 μm steps for selected cuboids from the affected set and highlights the importance of identifying and controlling proper measurement conditions. The fabrication of samples with a consistent height could lead to more consistent characterization. This could be realized by the identification of the proper target height per cuboid in an additional preceding sweep at the cost of increased fabrication time. IP-Dip samples were not affected by this issue, probably because their height variations were negligible when compared with the focal depth of the employed objective.

The expected correlation of the laser power with the E value was not found for IP-Q, with the E value rising with laser power at first, but then lowering again; see Fig. 4(d). A hypothesis for this behavior might be a partial detachment of the high dose specimen from the substrate, leading to an elastic contribution from between cuboid and substrate.

As the microindentation and Raman spectroscopy measurements are independent of this unexplained behavior, they show an expected trend of a rising DC value leading to a rising E value; see Fig. 5(b).

5 Conclusion

We performed a systematic study of the mechanical properties of polymer structures fabricated via TPP for the two specialized photoresists IP-Dip and IP-Q. For this purpose, parameter sweeps of cuboid polymer structures with variations of the laser power and scan speed were fabricated and characterized via Raman spectroscopy and micro- or nanoindentation.

We show the similarities and differences in the behavior of the two materials and compare the properties of IP-Dip with the literature. The characterized properties of IP-Q manifest as the current state of knowledge of the material. We confirm the transferability of the characterization process to other photoresists, although not without stating encountered issues and circumvention approaches. The link between the user's need for certain mechanical behavior and the measured Young's modulus starts with a program. In it, settings are posed; these affect the exposure dose, which affects the measurable DC, which affects Young's modulus. The programmable mechanical behavior is suitable for creating structures for applications like metagratings and metamaterials that require specific properties. Raman spectroscopy can then be used to validate the selected properties nondestructively by comparison with our findings.

Prospective cuboid fabrication will receive additional attention to the total height to make subsequent characterization more consistent and less prone to failure. Future work will investigate the modulation of hatch and slice distances to increase the addressable DC range.

Acknowledgments

This work was cofunded by the European Fund for Regional Development EFRE, the state of Brandenburg and the European Union grant reference number 85038023 and cofunded by the Federal Ministry of Education and Research (BMBF) under the project reference numbers 16FMD01K, 16FMD02, and 16FMD03. The authors have no competing interests to declare that are relevant to the content of this article. Study conception, study design, material preparation, data collection, and analysis were performed by Severin Schweiger, Tim Schulze, Peter Reinig, and Simon Schlipf. The first draft of the manuscript was written by Severin Schweiger, and all authors commented on previous versions of the manuscript. All authors read and approved the final manuscript.

Data, Code, and Material Availability

The code and datasets generated and analyzed during the current study are not publicly available due to confidentiality regulations but are available from the corresponding author upon reasonable request.

References

1. T. Baldacchini, *Three-Dimensional Microfabrication Using Two-Photon Polymerization*, William Andrew, an imprint of Elsevier, Norwich (2020).
2. J. Serbin, A. Ovsianikov, and B. Chichkov, "Fabrication of woodpile structures by two-photon polymerization and investigation of their optical properties," *Opt. Express* **12**, 5221–5228 (2004).
3. A. K. Ustun and J. Zou, "A photoacoustic sensing probe based on silicon acoustic delay lines," *J. IEEE Sens. J.* **21**, 21371–21377 (2021).
4. Z. Faraji Rad, P. D. Prewett, and G. J. Davies, "An overview of microneedle applications, materials, and fabrication methods," *Beilstein J. Nanotechnol.* **12**, 1034–1046 (2021).
5. M. J. Mirzaali et al. "Curvature induced by deflection in thick meta-plates," *Adv. Mater.* **33**, 2008082 (2021).
6. J. Bauer et al., "Programmable mechanical properties of two-photon polymerized materials: from nanowires to bulk," *Adv. Mater. Technol.* **4**, 1900146 (2019).
7. E. D. Lemma et al., "Mechanical properties tunability of three-dimensional polymeric structures in two-photon lithography," *IEEE Trans. Nanotechnol.* **16**, 23–31 (2016).
8. N. Rohbeck et al., "Effect of high strain rates and temperature on the micromechanical properties of 3D-printed polymer structures made by two-photon lithography," *Mater. Des.* **195**, 108977 (2020).
9. P. Golvari and S. M. Kuebler, "Fabrication of functional microdevices in SU-8 by multi-photon lithography," *Micromachines* **12**, 472 (2021).
10. I. S. Ladner et al., "Tensile properties of polymer nanowires fabricated via two-photon lithography," *RSC Adv.* **9**, 28808–28813 (2019).
11. L. J. Jiang et al., "Two-photon polymerization: investigation of chemical and mechanical properties of resins using Raman microspectroscopy," *Opt Lett.* **39**, 3034–3037 (2014).
12. G. M. Pharr and W. C. Oliver, "Measurement of thin film mechanical properties using nano-indentation," *MRS Bull.* **17**, 28–33 (1992).
13. T. Baldacchini and R. Zadoyan, "In situ and real time monitoring of two-photon polymerization using broadband coherent anti-Stokes Raman scattering microscopy," *Opt. Express* **18**, 19219–19231 (2010).
14. A. Melnikov et al., "Microacoustic metagratings at ultra-high frequencies fabricated by two-photon lithography," *Adv. Sci.* **9**(20) (2022).

15. S. Schweiger et al., "Two-photon lithography parameter study for manufacturing of acoustic metamaterials on MEMS," in *MST Kongress* (2021).
16. Nanoscribe GmbH & Co. KG, "MSDS IP-Q," EC No 1907/2006 (2020).
17. Nanoscribe GmbH & Co. KG, "IP-Photoresins," https://www.nanoscribe.com/en/products/ip-photoresins (accessed June 2022).
18. M. Göppert-Mayer, "Über Elementarakte mit zwei Quantensprüngen," *Ann. Phys.* **401**, 273–294 (1931).
19. S. Schweiger, S. G. Koch, and H. Schenk, "Two-photon-lithography substrate reflection and absorption compensation for additive manufacturing of metamaterials on MEMS," in *44th Int. Spring Semin.* (2021).
20. E. M. Harnisch, *Two-Photon Polymerization on Metal Surfaces for Structuring Moulding Tools*, Apprimus (2019).
21. S. K. Saha et al., "Effect of proximity of features on the damage threshold during submicron additive manufacturing via two-photon polymerization," *J. Micro Nano-Manuf.* **5**, 031002 (2017).
22. J. B. Mueller, J. Fischer, and M. Wegener, *Reaction Mechanisms and In situ Process Diagnostics*, Elsevier (2020).
23. L. E. S. Silva, A. A. Martin, and A. L. B. Pinheiro, "Degree of conversion of composite resin: a Raman study," *J. Clin. Laser Med. Surg.* **21**, 357–362 (2003).
24. J. S. Oakdale et al., "Post-print UV curing method for improving the mechanical properties of prototypes derived from two-photon lithography," *Opt. Express* **24**, 27077–27086 (2016).
25. W. C. Oliver and G. M. Pharr, "An improved technique for determining hardness and elastic modulus using load and displacement sensing indentation experiments," *J. Mater. Res.* **7**, 1564–1583 (1992).
26. DIN EN ISO 14577-1:2015-11, "Metallische Werkstoffe – Instrumentierte Eindringprüfung zur Bestimmung der Härte und anderer Werkstoffparameter – Teil 1: Prüfverfahren," ISO 14577-1:2015 EN ISO 14577-1:2015, Berlin.
27. L. R. Meza et al., "Resilient 3D hierarchical architected metamaterials," *Proc. Natl. Acad. Sci. U.S.A.* **112**, 11502–11507 (2015).
28. A. A. Bauhofer et al., "Harnessing photochemical shrinkage in direct laser writing for shape morphing of polymer sheets," *Adv. Mater.* **29**, 1703024 (2017).
29. J. Bauer et al., "Push-to-pull tensile testing of ultra-strong nanoscale ceramic-polymer composites made by additive manufacturing," *Extreme Mech. Lett.* **3**, 105–112 (2015).
30. A. Schroer et al., "Deformation behavior and energy absorption capability of polymer and ceramic-polymer composite microlattices under cyclic loading," *J. Mater. Res.* **33**, 274–289 (2015).

Severin Schweiger is a doctoral candidate at the Fraunhofer Institute for Photonic Microsystems in Dresden. He received his BEng degree in process and environmental engineering from the University of Applied Sciences Augsburg and his MSc degree in micro- and nanotechnology from the University of Applied Sciences Munich in 2013 and 2017, respectively. He is currently researching two-photon polymerization lithography and its effects on microelectromechanical systems.

Tim Schulze received his BS and MS degrees in physics from Humboldt University of Berlin in 2015 and 2018, respectively. Currently, he is pursuing his PhD in physics at Fraunhofer Institute for Photonic Microsystems and the Brandenburg University of Technology. His research interests include terahertz microcomponents, 4D microprinting, and near-infrared spectroscopy.

Simon Schlipf received his BS and MS degrees in physics from Eberhard Karls University of Tübingen in 2010 and 2016, respectively. He received his PhD in physics at Technical University of Dresden in 2021 for his work researching stress effects on the electrical performance of transistors. Currently, he is employed as an integration engineer at GlobalFoundries.

Peter Reinig received his diploma in physics from the University Oldenburg and his doctorate in physics from Philipps-University Marburg, in 1997 and 2002, respectively. He worked on thin film materials for photovoltaics at Helmholtz–Zentrum Berlin and has >10 years industrial

experience in the field of optical metrology for semiconductor manufacturing at Infineon Technologies and Photovoltaics at SGS. His research interests at Fraunhofer IPMS since 2013 are in the area of MEMS-based photonic sensing for environmental and medical applications.

Harald Schenk studied physics and submitted his dissertation in the field of electrical engineering in 1997. At the Fraunhofer Institute for Photonic Microsystems, he became department head and deputy director in 2002 and 2004, respectively. In 2012, he launched the MESYS project group and has since held the professorship for micro- and nanosystems at BTU Cottbus-Senftenberg. He has been heading the IPMS together with Prof. Dr.-Ing. Hubert Lakner since 2013.